# Remote control of regioselectivity in acyl-acyl carrier protein-desaturases

Jodie E. Guy[a], Edward Whittle[b], Martin Moche[c], Johan Lengqvist[d,1], Ylva Lindqvist[a,2], and John Shanklin[b,2]

[a]Department of Medical Biochemistry and Biophysics, Molecular Structural Biology, Karolinska Institutet, Tomtebodavägen 6, S-171 77 Stockholm, Sweden; [b]Department of Biology, Brookhaven National Laboratory, Upton, NY 11973; [c]Department of Medical Biochemistry and Biophysics Structural Genomics Consortium, Karolinska Institutet, S-171 77 Stockholm, Sweden; and [d]Department of Medical Biochemistry and Biophysics, Chemistry I, Karolinska Institutet, S-171 77 Stockholm, Sweden

Edited* by Chris R. Somerville, University of California, Berkeley, CA, and approved August 8, 2011 (received for review June 24, 2011)

**Regiospecific desaturation of long-chain saturated fatty acids has been described as approaching the limits of the discriminatory power of enzymes because the substrate entirely lacks distinguishing features close to the site of dehydrogenation. To identify the elusive mechanism underlying regioselectivity, we have determined two crystal structures of the archetypal Δ9 desaturase from castor in complex with acyl carrier protein (ACP), which show the bound ACP ideally situated to position C9 and C10 of the acyl chain adjacent to the diiron active site for Δ9 desaturation. Analysis of the structures and modeling of the complex between the highly homologous ivy Δ4 desaturase and ACP, identified a residue located at the entrance to the binding cavity, Asp280 in the castor desaturase (Lys275 in the ivy desaturase), which is strictly conserved within Δ9 and Δ4 enzymes but differs between them. We hypothesized that interaction between Lys275 and the phosphate of the pantetheine, seen in the ivy model, is key to positioning C4 and C5 adjacent to the diiron center for Δ4 desaturation. Mutating castor Asp280 to Lys resulted in a major shift from Δ9 to Δ4 desaturation. Thus, interaction between desaturase side-chain 280 and phospho-serine 38 of ACP, approximately 27 Å from the site of double-bond formation, predisposes ACP binding that favors either Δ9 or Δ4 desaturation via repulsion (acidic side chain) or attraction (positively charged side chain), respectively. Understanding the mechanism underlying remote control of regioselectivity provides the foundation for reengineering desaturase enzymes to create designer chemical feedstocks that would provide alternatives to those currently obtained from petrochemicals.**

diiron enzyme | enzyme redesign | lipid metabolism | enzyme mechanism

Acyl-acyl carrier protein (ACP) desaturases are a family of diiron center containing soluble enzymes that introduce double bonds into acyl-ACPs in an oxygen-dependent reaction. In plants, acyl-ACP desaturases play a key role in biosynthesis of monounsaturated fatty acids, acting as the primary determinant for the composition of unsaturated fatty acids in plant membranes and seed oils. A striking feature of the reaction catalyzed by these enzymes is that it is performed with extremely high stereo- and regioselectivity, despite the fact that the substrates are composed of essentially equivalent methylene chains that completely lack distinguishing landmarks close to the site of desaturation. As Nobel Prize winner Konrad Bloch observed in 1969, "The stereospecific removal of hydrogen in the formation of oleate, although predictable on principle grounds would seem to approach the limits of the discriminatory power of enzymes" (1).

We have a long-standing interest in identifying the bases of this discriminatory power of desaturases. Acyl-ACP desaturases are Δ counters—i.e., they insert a double bond a certain number of carbons from the carboxyl end of the fatty acid (2). A detailed understanding of how this counting occurs could enable reengineering of desaturases to introduce double bonds at desired locations within the fatty acid substrate. Such enzymes would be highly desirable in biotechnological applications to produce designer fatty acids for use as feedstocks for a variety of applications, including the production of polymers (3). However, 40 y after Bloch's quote, the mechanisms of regioselectivity in the desaturases remain largely unexplained, in part because the search for contributing factors cannot be localized to the active site.

In 1996, we solved the structure of the archetypal Δ9-stearoyl-ACP desaturase from *Ricinus communis* (castor) (4), which introduces a *cis* double bond in ACP-bound 18:0 to produce 18:1Δ9 (5). The crystal structure showed the desaturase to be a homodimeric protein with a conserved four-helix bundle, containing the diiron active site, at the core of each monomer. The structure also revealed a substrate-binding cavity capable of binding the acyl chain in an extended configuration, within which a "boomerang-shaped" bend imparts an eclipsed substrate conformation, consistent with the observed pro-*R* pro-*R* dehydrogenation (6) which leads to the formation of the *cis* double bond. Although this structure explained the mechanism of stereoselectivity, the determinants of regioselectivity remained elusive. The isolation of genes encoding a series of soluble desaturases with distinct regioselectivity presented an opportunity to perform comparative structural studies. However, the crystal structure of the ivy Δ4–16:0-desaturase revealed it to be extremely similar to that of the castor desaturase; the two structures superimpose with $C^{\alpha}$ rmsd of 0.76 Å over 311 amino acids (7). Whereas some clusters of sequence variation are seen to correspond to chain-length specificity, such as the residues lining the bottom of the substrate-binding cavity, in general, sequence variations appear dispersed throughout the body of the protein and a comparison of the desaturase structures provided no clear indication as to what might explain a five-carbon shift in regioselectivity. Moreover, both castor and ivy desaturase maintain their in vivo regioselectivity when assayed with the same spinach ACP substrates, implying that the nature of the interaction between the ACP and the desaturase enzyme may differ for the two desaturases. We therefore initiated studies on the desaturase–ACP complex in order to address the question of regioselectivity. Here we present crystal structures of castor desaturase in complex with acyl-ACP. Analysis of these structures in combination with modeling experiments allowed us to formulate the hypothesis that Asp 280 of the castor desaturase, corresponding to Lys275 in the ivy enzyme, is a key determinant of ACP binding and regioselectivity. Biochemical analysis

Author contributions: Y.L. and J.S. designed research; J.E.G., E.W., M.M., J.L., Y.L., and J.S. performed research; E.W. and M.M. contributed new reagents/analytic tools; J.E.G., E.W., M.M., J.L., and Y.L. analyzed data; and J.E.G., Y.L., and J.S. wrote the paper; .

The authors declare no conflict of interest.

*This Direct Submission article had a prearranged editor.

Data deposition: The desaturase–acyl carrier protein complexes have been deposited in the Protein Data Bank, www.pdb.org (PDB ID codes 2XZ0 and 2XZ1).

[1]Current address: Safety Assessment, Molecular Toxicology, AstraZeneca R&D, 15185 Södertälje, Sweden.

[2]To whom correspondence may be addressed. E-mail: Ylva.Lindqvist@ki.se or shanklin@bnl.gov.

This article contains supporting information online at www.pnas.org/lookup/suppl/doi:10.1073/pnas.1110221108/-/DCSupplemental.

of a series of site-directed mutants provides compelling support for this hypothesis.

## Results and Discussion

With 18 and 16 carbon substrates, the castor desaturase exhibits exclusively Δ9 desaturation and with 14:0—predominantly Δ9, but with a minor fraction (17%) of Δ4 desaturation (Table S1). In contrast, the ivy desaturase exhibits exclusively Δ4 selectivity with 14 and 16 carbon substrates but, surprisingly, with 18 carbon substrate displays almost exclusively (97%) Δ9 desaturation. We previously solved the crystal structures of these two desaturases, the Δ9–18:0-ACP desaturase from castor (4) and the Δ4–16:0-ACP desaturase from ivy (8). The two structures were very similar, as predicted by the 76% amino acid sequence identity, and a detailed comparison yielded few insights into the basis for their different regioselectivities, which involves a shift in register of five carbons on the acyl chain with respect to the diiron active site. We therefore focused on solving the crystal structures of these desaturases with their acyl-ACP substrates as an approach to understand regioselectivity.

**Synthesis and Validation of the Acyl-ACP–Castor Δ9 Desaturase Complex.** Previous work has shown that chemical reduction of the desaturase results in tight and stoichiometric binding of its acyl-ACP substrate (9). We therefore produced the $4e^-$ reduced desaturase–acyl-ACP complex under anaerobic conditions and purified the resulting complex. To assess the stoichiometry of the castor desaturase:acyl-ACP complex, it was analyzed by electrospray mass spectrometry under nondenaturing conditions, which shows one major peak envelope in the 4,300–5,500 $m/z$ range (Fig. S1). Deconvolution of the 4,300–5,350 $m/z$ range yielded an observed molecular mass of 102,556 Da (Fig. S1, *Inset*), 152-Da (0.15%) higher than the calculated mass of the complex, likely reflecting the presence of two unknown metal ions, which we identify bound to desaturase in the dimer interface in the crystal structure. By collision-induced dissociation, this complex could be fragmented and its monomeric/dimeric constituents identified. That the 4,300–5,500 $m/z$ envelope is the major ion species observed shows that the 2:2 complex of desaturase:stearoyl-ACP is the predominant species in solution.

**Nature of the Complex in the Crystals.** The complex between castor desaturase and acyl-ACP was crystallized under two separate conditions. Despite the fact that all protein used for crystallization contained a predominantly 2:2 (desaturase:acyl-ACP) complex, in the asymmetric unit of crystal form 1 there are three subunits of desaturase and only a single subunit of stearoyl-ACP. Desaturase subunits A and B form the biological dimer with stearoyl-ACP bound only to subunit B (i.e., forming a 2:1 complex). Subunit C forms a dimer with its crystallographic twofold symmetry-related mate without ACP bound to either partner. In contrast, in crystal form 2, the asymmetric unit contains the expected one desaturase dimer with two bound ACP molecules. A cartoon representation of the fully occupied structure is shown in Fig. 1*A*. Although the 2:1 dimer seen in crystal form 1 appears to be a result of crystal packing constraints, Broadwater et al. previously suggested that a complex with 2:1 stoichiometry could be functionally significant (9) and they hypothesized that the use of alternating active sites in the desaturase dimer could enable coordination of the transfer of reducing equivalents, substrate binding, and product release. It is also reported that binding of the first ACP to the desaturase dimer occurs with a 30-fold higher affinity than binding of the second ACP (10). This is consistent with our structures because even the 2:2 dimer of crystal form 2 contains one well-ordered ACP (chain C) and a second more poorly ordered ACP (chain D).

**Structure of the Desaturase in the Acyl-ACP–Castor Desaturase Complex.** The overall structure of the desaturase in the two crystal forms is almost identical, with rmsd of 0.5 Å between the subunits and is essentially the same as that of the free enzyme, apart from residues 336–347, which are disordered in all structures of the free enzyme but ordered in the complex. The desaturase diiron center appears to be oxidized, with iron–iron distances of between 3.0 and 3.3 Å in all subunits of both crystal forms, in contrast to previous structures of the castor desaturase in which the iron centers were reduced (5, 11). The positions of the iron ions are almost identical to those seen in the oxidized ivy desaturase crystal structure (7), although no electron density is observed for the expected μ-oxo bridge. In both crystal forms, some additional density is seen adjacent to the iron ions in the active site, but too far from the irons to be the bridging oxygen. In crystal form 1, this density is described as a water molecule, but in crystal form two, the density is too strong to be attributed to water and was ultimately modeled as a cacodylate ion. In both crystal forms, density for two partially occupied metal ions is seen on the desaturase dimer interface, coordinated by the side chains of Glu106, and they were modeled as zinc and calcium in crystal forms 1 and

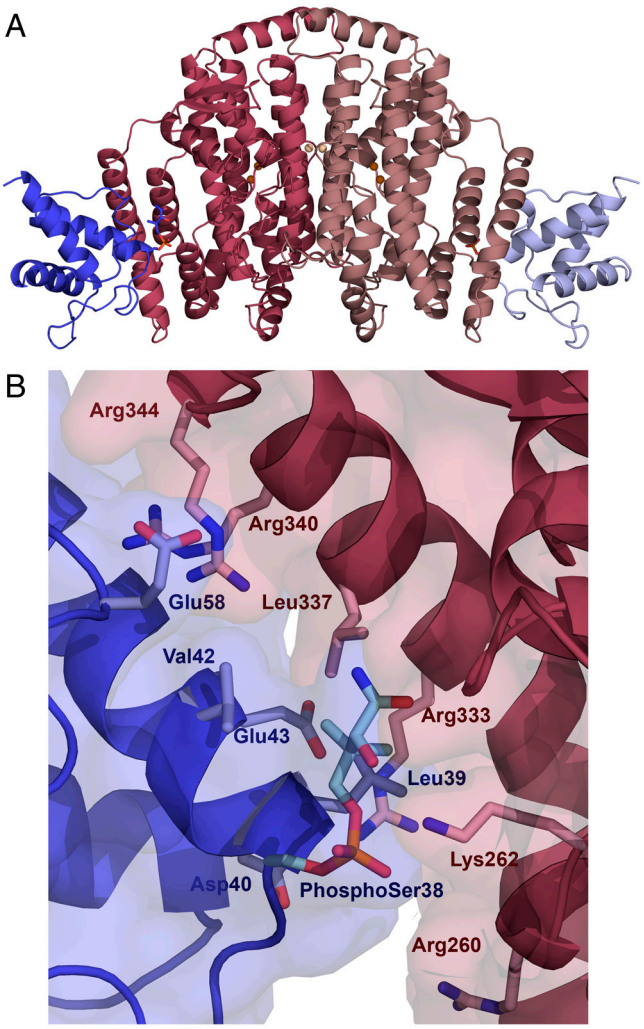


**Fig. 1.** The desaturase–ACP complex structure. (*A*) Fully occupied complex of crystal form 2 in cartoon representation. The desaturase monomers are colored in dark and light pink, and the ACP in dark and light blue. The defined portions of the phospho-serine and pantetheine linkage are depicted as stick representations, and the catalytic irons are shown as brown spheres with the metal ions on the dimer interface in light brown. (*B*) The desaturase–ACP interface in crystal form 2, with the desaturase chain B (pink) and the ACP chain C (blue). Residues participating in the desaturase–ACP interaction are shown in stick representation, with the phospho-serine38 and the defined part of the pantetheine chain depicted in pale blue.

2, respectively, due to the presence of these metals in X-ray fluorescence emission spectra recorded from the crystals.

**Structure of ACP in the Complex.** The structure of desaturase-bound ACP is very similar to the previously published NMR structures of spinach ACP. A DALI (12) search with chain C of crystal form 2 gives the top match as Protein Data Bank (PDB) ID 2FVF, the NMR structure of decanoate bound ACP, with an rmsd of 1.4 Å across all $C^{\alpha}$ atoms. The three ACP molecules (chain D in crystal form 1, chains C and D in crystal form 2) superimpose with pairwise rmsd values of 0.7–1.2 Å; the only significant differences are found in the long loop between residues Leu17 and Asp37. This loop (particularly residues 22–28) is involved in extensive crystal packing interactions in chain C of crystal form 2, which could explain both the different conformations of the loops and the fact that this chain has much higher quality electron density despite the lower nominal resolution of crystal form 2. Of the 4′-phosphopantetheine group attached to Ser38, only the phosphate group and the region up to the first amide group is defined in electron density in subunit C, and only the phosphate group in chain D and in crystal form 1. Unfortunately, no convincing electron density is observed for the remainder of the pantetheine group or for the fatty acid.

**Interaction Between Stearoyl-ACP and Desaturase.** Examples of the electron density on the desaturase–ACP interface of each structure are shown in Fig. S2. Due to the higher quality of chain C of crystal form 2, analysis of the interface is based on the interaction between this chain and its bound desaturase, chain B. The desaturase–ACP interface, as measured with the PISA (13) server at the European Bioinformatics Institute, comprises approximately 500 $Å^2$, representing 8.4% of the available surface area of ACP and 3.2% of the available surface area of the desaturase. ACP contributes negatively charged residues and the desaturase has predominantly positively charged residues on the interaction surface (Figs. 1*B* and 2). Seven desaturase residues, Arg260 and Lys262 from the C terminus of α8 as well as Arg333, Arg336, Leu337, and Arg340 from the long helix α11 and Arg344 from the following loop, comprise the largest portion of the ACP interaction surface (Figs. 1*B* and 2). Residues 336–347 are in a region of the structure that was very poorly defined in the free desaturase structure, indicating high flexibility, but is well-ordered in the complex. In ACP, residues from helix 2—the recognition helix (39–52), Asp37, phospho-Ser38 from the preceding turn, and Glu58—constitute the main part of the interface. The side chain of Lys262 from the desaturase makes a salt bridge to a phosphate-oxygen of phospho-Ser38 in ACP carrying the pantetheine group. Lys262 is a Ramachandran outlier both in the two complex structures and in free desaturase. Arg333 of the desaturase is interacting with the ACP residues Glu43 and Asp 40, and Arg340 interacts with ACP residue Glu49. Arg344 of the desaturase is positioned very close to Glu58 of the ACP but the density for the two side chains is not clear enough to be certain that they interact. Very little hydrophobic interaction is seen between the two proteins, although Leu337 of the desaturase and Leu39 of the ACP are facing each other at a distance of 4 Å. The three interfaces B:C, A:D, and that in crystal form 1 are not identical; small differences arise due to slightly different orientations of the ACP relative to desaturase in each case, indicating a plasticity in the interaction (Fig. S3*B*).

Four of the amino acid side chains that constitute the ACP-interacting surface within the castor desaturase–ACP crystal structure differ between Δ4 and Δ9 desaturases. We therefore constructed the quadruple mutant Arg333Lys, Leu337Val, Arg340Lys, Arg344Lys in which the side chains of the castor Δ9 desaturase were replaced by the equivalent side chains present in

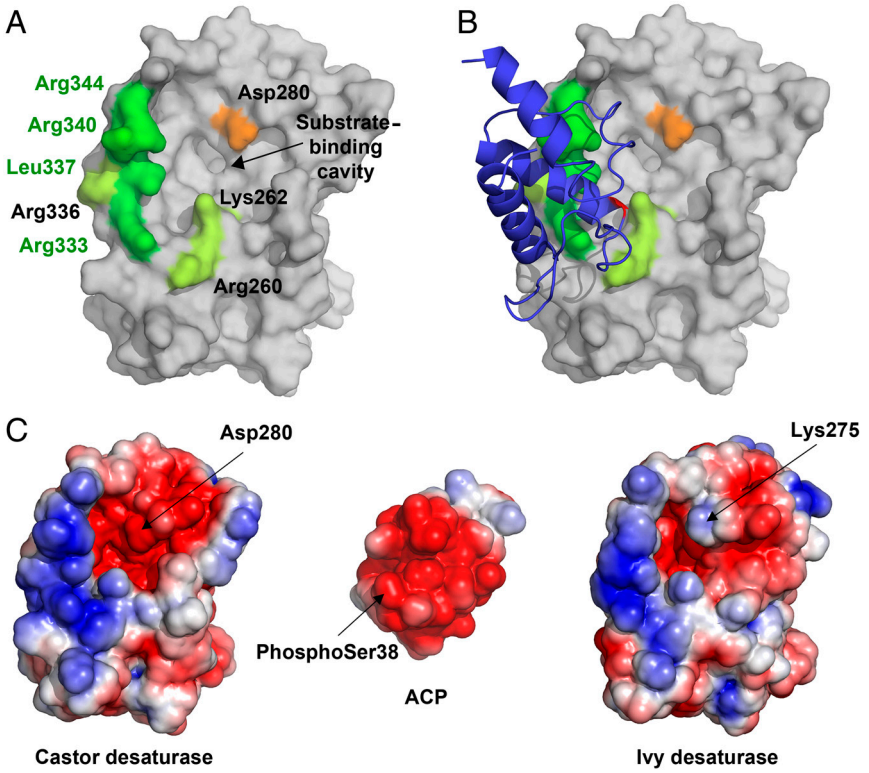


**Fig. 2.** The desaturase–ACP interaction surface. (*A*) Surface view of the castor desaturase, looking directly at the entrance to the substrate-binding cavity. Desaturase residues that interact with ACP in the complex are colored green, with those that differ between ivy and castor and comprise the "quadruple mutant" highlighted in bright green. Asp280 is highlighted in orange. (*B*) The same as *A*, but with ACP added as a cartoon. The ACP is colored blue, with phospho-serine38 highlighted in red. (*C*) The electrostatic surface potentials of the desaturase–ACP interaction site. The desaturases are shown in the same orientation as *A* and *B* while ACP is rotated 180° with respect to *B* to show the interaction surface.

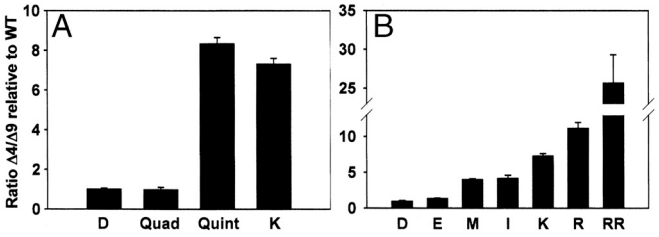


**Fig. 3.** Regioselectivity of various mutants relative to castor WT (D) Δ9 desaturase with 14:0-ACP substrate. (*A*) The regioselectivity of the quadruple mutant (Arg333Lys, Leu337Val, Arg340Lys, Arg344Lys). The quintuple mutant is the quadruple mutant plus Asp280Lys (K), and the single mutant Asp280Lys (K) is also shown. (*B*) A comparison of the regioselectivity for WT (D) and substitutions as indicated at position 280, Glu (E), Met (M), Ile, (I), Lys (K), Arg (R), and the double mutant Asp280Arg, Ala284Arg (RR).

Δ4 desaturases. As seen in Fig. 3*A*, this mutant showed no change in regioselectivity relative to the castor WT enzyme. This is consistent with analysis of the ivy desaturase used for crystallography which maintained its Δ4 desaturation when its C-terminal 38 amino acids were substituted with that of the castor desaturase (which included three of the four residues that differ between Δ4 and Δ9 desaturases in the desaturase–ACP interface) (7). All subsequent mutations in this work were made to the castor desaturase because it has higher in vitro activity than the ivy enzyme and we have crystallographic data of the castor enzyme in complex with ACP to serve as a guide.

**Modeling the Acyl Chain in the Caster Complex Structure Places C9 and C10 Optimally for Δ9 Desaturation.** As described above, presence of the full desaturase–acyl-ACP complex used for crystallization was validated in solution by mass spectrometry, but although the resulting crystal structures have clear density for the desaturase and ACP moieties, the majority of the pantetheine and fatty acid are not visible. Thus, although the complex structure provides a detailed description of a desaturase–ACP interface, it does not provide many clues as to the mechanism of regioselectivity. The structure of the substrate-binding cavity only allowed us to model the pantetheine arm and the acyl chain in extended conformation, placing C9 and C10 adjacent to the diiron site at which an $O_2$-derived iron-bound oxidant abstracts two hydrogens to form the incipient double bond (Fig. 4*A*) precluding other sites of desaturation.

However, to achieve Δ4 desaturation of 16:0-ACP, C4 and C5 must be positioned adjacent to the catalytic diiron center, implying that the acyl chain must be inserted five carbons deeper into the substrate-binding channel and, despite the shorter length of the fatty acid, an extra three carbon atoms must be accommodated in the base of the substrate-binding cavity. This second point is explained because we previously identified a cluster of amino acid substitutions and altered side-chain positions in the base of the substrate-binding cavity which, when compared to the 18:0-Δ9 castor enzyme, could accommodate the three additional carbons (7). However, the distance between phospho-Ser38 of the ACP and the diiron active site in the castor ACP–desaturase complex is too long to be bridged by the pantetheine group and the first four carbons of the acyl chain, implying that other binding modes for acyl-ACPs, in which phospho-Ser38 becomes positioned closer to the active site cavity, must occur. The small desaturase–ACP interface, involving predominantly electrostatic interactions between a positively charged patch on the desaturase and a negatively charged surface of ACP, could potentially accommodate different relative binding orientations. Small variations in ACP binding orientations in the three complex structures described herein support this idea (Fig. S3).

**Docking of ACP to the Ivy Desaturase Identifies an Alternative Binding Mode.** To explore the possibility of other binding modes of ACP, we performed modeling using the protein–protein interaction server Haddock (14) with ACP and castor or ivy desaturase. The results are presented in Table S2. A number of different ACP–desaturase binding modes were suggested by the program, although many could be discounted because phospho-Ser38 of the ACP moiety points away from the substrate-binding cleft. With the castor enzyme, we reproduced the crystal structure of the ACP complex (all other computed binding orientations of ACP being inconsistent with catalytically competent complexes). With the ivy enzyme, we also obtained an orientation of ACP approximating our crystal structure of the castor enzyme complex, consistent with the enzymes ability to catalyze Δ9 desaturation of 18:0-ACP and to further desaturate Δ9 16:1 or Δ9 18:1 to the corresponding Δ4,9-dienes, which is not surprising considering that residues in this interface are conserved or contain very conservative substitutions (Table S3). However, a different orientation, where the ACP phospho-Ser38 interacts with Lys275 (corresponding to Asp280 in the castor enzyme) at the entrance to the active site cavity was obtained (Table S2). This orientation

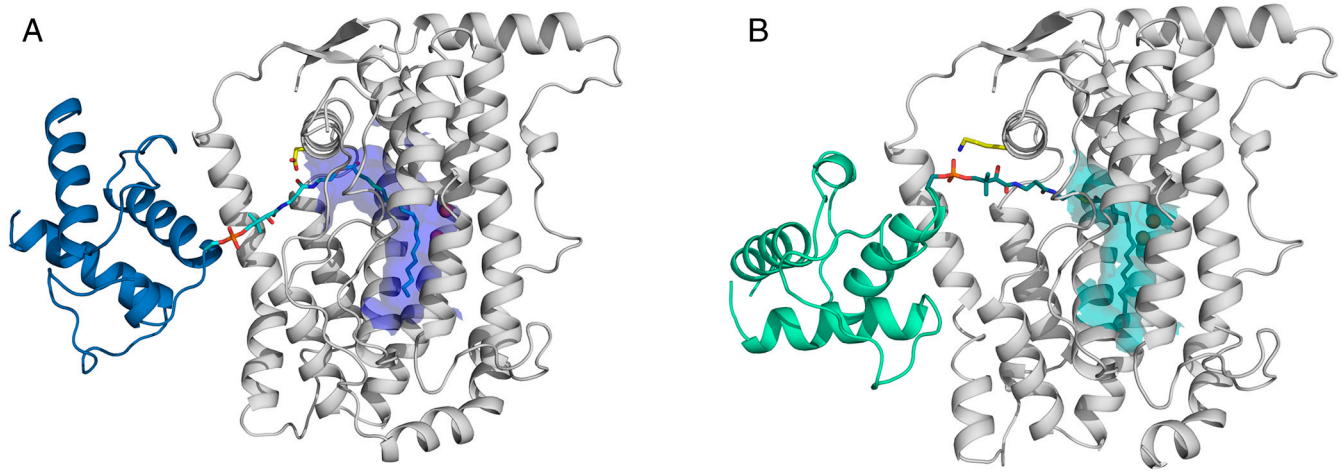


**Fig. 4.** Models of the complete desaturase–ACP complexes. (*A*) Castor desaturase–ACP complex (desaturase in gray and ACP in blue), with the modeled pantetheine and fatty acid (cyan) in stick representations. Residue Asp280 is highlighted in yellow, and the surface of the substrate-binding cavity (carved around the fatty acid) is depicted in blue. (*B*) The modeled ivy desaturase–ACP complex (desaturase in gray and ACP in green), with the modeled pantetheine and fatty acid (dark teal) in stick representations. Residue Lys275 is highlighted in yellow and the surface of the substrate-binding cavity (carved around the fatty acid) is shown in teal.

of ACP could precisely orient the acyl chain for Δ4 desaturation of 16:0 (Fig. 4*B*) with the previously reported pro-*R* pro-*R* enantioselectivity (15). Using the castor enzyme, with Asp280 exchanged for a lysine residue in the modeling, gave the same approximate orientation, which prompted us to probe the potential role of Asp280 for regioselectivity.

**Position 280 of the Castor Desaturase Has a Strong Influence on Regioselectivity.** Asp 280, the castor residue that corresponds to Lys275 in the ivy structure, is at the entrance to the substrate-binding cavity and its identity tracks with Δ4 or Δ9 regioselectivity. That the residue occupying this location in ivy desaturase, Lys275, was implicated in interacting with the phosphate of the pantetheine group of the computationally docked model of the ivy–ACP complex prompted us to add this residue to the previously described quadruple mutant to make castor quintuple mutant Asp280Lys, Arg333Lys, Leu337Val, Arg340Lys, Arg344Lys. As shown in Fig. 3*A*, this mutant exhibited an 8.3-fold increase in Δ4 desaturation relative to the castor WT. We therefore engineered the Asp280Lys single mutant to determine its contribution to the change in regioselectivity observed for the quintuple mutant, and show that it practically accounts for all of the change (Fig. 3*A*). This large switch in regioselectivity is consistent with the interaction of the phosphate group of phospho-Ser38 of the ACP moiety with Lys275 of the ivy enzyme proposed in the docking model of the ivy desaturase and ACP described above. To further test this modeled interaction, we evaluated the activity of Asp280Glu and Asp280Arg mutants. Substitution of the aspartate with glutamic acid resulted in a negligible change in regioselectivity, whereas substitution of the negatively charged Asp280 side chain with the positively charged arginine side chain resulted in a comparable change in regioselectivity to that observed for the lysine substitution (Fig. 3*B*). Consistent with these data, substitution of Asp280 for the neutral uncharged side chains methionine and isoleucine resulted in an intermediate level of regioselectivity change (Fig. 3*B*). These data suggest that the presence of negatively charged residues at position 280 of the castor enzyme repel the negatively charged phosphate group of phospho-Ser38, which favors ACP binding to the desaturase in the manner observed in the crystal structure. In this favored binding mode, the combined length of the pantetheine group and fatty acid in the extended configuration is consistent with Δ9 desaturation. However, upon substitution of the negatively charged Asp280 side chain with positively charged side chains, which can interact with the negatively charged phospho-Ser, binding of the ACP occurs in a manner consistent with that modeled for the ivy–ACP complex in which the ACP binding position would allow deeper insertion of the acyl chain into the substrate-binding cavity permitting Δ4 desaturation. The presence of a neutral side chain at position 280 of the castor enzyme would provide neither repulsion nor attraction and so neither ACP binding mode would be favored, leading to the observed change in regioselectivity of approximately fourfold. Because WT castor desaturase (containing Asp280) has a Δ9 : Δ4 ratio of 4.9:1, a change of approximately fourfold would bring that ratio close to unity, meaning neither Δ9 nor Δ4 mode is favored. Although the Arg280 mutant shows an 11.2-fold improvement in Δ4 to Δ9 specificity, it possesses some residual Δ9 desaturation. We therefore created a double mutant Asp280Arg, Ala284Arg, that introduces a second positive charge, at the opening of the cavity to test the hypothesis that additional positive charge should enhance interaction with phosophoser 38 of ACP and thereby enhance the Δ4 binding mode. The double mutant showed a 25.7-fold shift in Δ4 to Δ9 specificity relative to WT (Fig. 3*B*), consistent with this hypothesis. With the exception of Asp280Ala, the $k_{cat}$ of the single amino acid mutants were either equivalent to (Asp280Glu, Met, and Ile) or significantly higher than (Asp280Arg, Lys) that of the of the WT castor enzyme (*ca.* 0.4 $min^{-1}$) and, interestingly, the Asp280Arg, Ala284Arg double mutant showed the largest (*ca.* fivefold) increase relative to WT (Fig. S4).

Residue 284 is situated such that a lysine side chain at this position could interact with the phospho-Ser of the ACP in a manner very similar to that predicted for a lysine at position 280. The identification of a prime determinant of regioselectivity 27 Å from the diiron site, at which double-bond formation occurs, is perhaps surprising, however, that regioselectivity can be affected by interaction of the acyl carrier moiety and desaturase is not without precedent. Within the evolutionarily distinct class of integral membrane enzymes, the FAD5 desaturase was shown to perform Δ7 desaturation when presented with 16:0 esterified to monogalactosyldiacylglycerol, but Δ9 desaturation when presented with 16:0 esterified to phosphatidyl choline (16). Thus, for both soluble and integral membrane desaturase, regioselectivity is controlled remotely, albeit by different mechanisms. For the acyl-ACP desaturases, a change in charge of a single side chain results in a change in regioselectivity with the same acyl-ACP substrate, whereas for FAD5, a change in the charge of the substrate head group results in changes in regioselectivity with the same enzyme.

In summary, we demonstrate that residue 280 is the seminal determinant for the different binding modes of ACP with respect to the castor and ivy desaturase, predisposing the potential insertion depth of the acyl chain. The precise shape and depth of the cavity below the diiron site provide additional constraints that contribute to the extremely high fidelity of product regioselectivity observed for these enzymes. Using the knowledge presented herein as a basis for enzyme redesign, it is feasible that mutants of acyl-ACP desaturases, ACP, or perhaps both could be designed to create new binding modes, and combined with variations in the substrate-binding cavity below the diiron active site, could yield new regioselectivities and chain-length selectivities. Such enzymes could be used for the metabolic engineering of production plants in a similar fashion to that shown by Nguyen et. al. (17), for ω-7 fatty acids, to produce designer fatty acids that could constitute improved feedstocks for industry. These would be renewable and could serve as alternatives to feedstocks currently obtained from petrochemicals.

## Materials and Methods

**Complex Synthesis Purification and Validation.** Expression and purification of the mature castor desaturase protein and stearoyl-ACP were performed as previously described (18, 19). We prepared a 2:2 peroxodiferric–desaturase complex under anaerobic conditions as previously described (9). The reaction mixture was applied to a 260 mL TSKgel 3000SW column (Mac Mod Analytical) to separate desaturase complex from excess acyl-ACP. A sample of the complex was dialyzed against ammonium acetate to a final concentration of 10 pmol/μL and analyzed on a quadrupole-orthogonal acceleration time-of-flight, Q-TOF1 mass spectrometer (Micromass Corp.) equipped with the Z-spray electrospray source and optimized for the detection of noncovalent complexes (Fig. S1).

**Complex Crystallization and Structure Determination.** Crystals of crystal form 1 were grown in hanging drops at 4 °C. The desaturase–stearoyl-ACP complex was at a concentration of 6–8 mg/mL in 70 mM NaCl and 20 mM Hepes buffer (pH 7.0). The protein solution was mixed (2 + 2 μL) with a well solution containing 4–5% (wt/vol) PEG 20,000, 8% (vol/vol) PEG 550 monomethyl ether, 180 mM sodium bromide, 0.1 M sodium acetate (pH 5.62), and 15% (vol/vol) glycerol. Data from this crystal form was collected at beamline X11 in Deutsches Elektronen-Synchrotron, Hamburg, from a cryocooled crystal at a wavelength of 0.811 Å. The X-ray data were processed with MOSFLM (20) and SCALA (21) from the CCP4 suite (22). The cell parameters in space group $P3_121$ were determined to be $a = b = 188.3$ Å and $c = 81.3$ Å. Crystals of crystal form 2 were grown in sitting drops at 4 °C from a 8–10 mg/mL concentration of desaturase-19:0 ACP complex in 70 mM NaCl and 20 mM Hepes buffer (pH 7.0). The well solution contained 16–20% 2-methyl-2,4-pentanediol, 6–8% PEG 20,000, 0.1 M sodium cacodylate (pH 5.8), and 4–6% acetonitrile. The drop was formed from 1 μL of protein solution mixed with an equal volume of the well solution. Data were collected from a cryocooled crystal on beamline ID23-2 at the European Synchrotron Radiation Facility,

France. X-ray data were processed with MOSFLM and SCALA from the CCP4 suite. The cell parameters in space group $P4_322$ were determined to be $a = b = 76.4$ Å and $c = 403.4$ Å. The structures were solved by molecular replacement using the program MOLREP (23), with the original castor desaturase structure (1AFR) and an NMR structure of spinach ACP (PDB ID 2FVE) as search models. Restrained refinement was performed with REFMAC5 (24) using either individual (crystal form 1) or group (crystal form 2) B-factor refinement. Translation, libration, screw (TLS) refinement (one TLS group per chain) was implemented in the later stages. In order to maximize the data-to-parameter ratio, the structure of the desaturase was initially fixed and only the ACP refined; the desaturase was included in the later stages of refinement. Tight noncrystallographic symmetry restraints were used throughout refinement wherever possible, and simulated-annealing composite omit maps, calculated in CNS (25), were utilized in model building to minimize model bias. Model building was performed in COOT (26). Accuracy of the models was assessed using PROCHECK (27), SFCHECK (28), and MolProbity (29). Data and refinement statistics for each structure are summarized in Table S4. Model coordinates and experimental data have been deposited in the PDB, with PDB IDs 2XZ0 for crystal form 1 and 2XZ1 for crystal form 2. Figures for the manuscript were prepared using PyMOL (30).

**Molecular Modeling.** The modeling of ACP–desaturase complexes were performed using the Haddock easy interface server (http://haddock.chem.uu.nl/) (14). HADDOCK distinguishes itself from ab initio docking methods in that it uses information from identified or predicted protein interfaces to drive the docking process. Thus, with different starting suggestions for interacting residues, different solutions will be obtained. The resulting complexes are clustered and scored based on the weighted sum of various energy terms (e.g., buried surface area, electrostatic energy, van der Waals energy). Because the program does not recognize the phospho-serine residue, it was modeled as a glutamic acid in the Haddock procedure. The pantetheine and fatty acid thioester moieties were manually fitted in the active site and regularized in COOT.

**Mutagenesis and Activity Assays.** The construction of mutant Asp280Lys was previously described (31) and the other Asp280 mutants were made using the same approach. Mutant Asp280Ala was further mutagenized to convert Ala284 to either an Asp or Lys. Fatty acid desaturase reactions were performed by incubation of the desaturase with 14:0-ACP substrate in the presence of recombinant spinach ACP-I (32) as previously described (31, 33). Fatty acid methyl esters (FAMEs) were prepared by addition of 2 mL of 1% $NaOCH_3$ in methanol and incubation for 60 min at 50 °C, after which the mixture was acidified with glacial acetic acid and the FAMEs extracted into hexane. The hexane was evaporated by incubation at room temperature overnight to a final volume of approximately 100 μL in preparation for GC analysis. Analysis was performed with the use of an HP5973 gas chromatograph-mass spectrometer (Hewlett-Packard) fitted with 60-m × 250-μm SP-2340 capillary columns (Supelco) as previously described (31). Assignments of double-bond position were based on elution times of methyl esters and identities confirmed by MS analysis of dimethyl disulfide derivatives, performed as previously described (34).

**ACKNOWLEDGMENTS.** We thank The Swedish Foundation for International Cooperation in Research and Higher Education and the Swedish Research Council for financial support to Y.L. and the Office of Basic Energy Sciences of the US Department of Energy to E.J.W. and J.S. We gratefully acknowledge the European Synchrotron Radiation Facility, MAX-Lab, Lund, and the European Molecular Biology Laboratory Hamburg Outstation at Deutsches Elektronen-Synchrotron, and the National Synchrotron Light Source at Brookhaven National Laboratory for beam time allocation.

1. Bloch K (1969) Enzymatic synthesis of monounsaturated fatty acids. *Acc Chem Res* 2:193–202.
2. Shanklin J, Cahoon EB (1998) Desaturation and related modifications of fatty acids. *Annu Rev Plant Physiol Plant Mol Biol* 49:611–641.
3. Shanklin J (2000) Exploring the possibilities presented by protein engineering. *Curr Opin Plant Biol* 3:243–248.
4. Shanklin J, Somerville C (1991) Stearoyl-acyl-carrier-protein desaturase from higher plants is structurally unrelated to the animal and fungal homologs. *Proc Natl Acad Sci USA* 88:2510–2514.
5. Lindqvist Y, Huang W, Schneider G, Shanklin J (1996) Crystal structure of a delta nine stearoyl-acyl carrier protein desaturase from castor seed and its relationship to other diiron proteins. *EMBO J* 15:4081–4092.
6. Behrouzian B, Savile CK, Dawson B, Buist PH, Shanklin J (2002) Exploring the hydroxylation-dehydrogenation connection: Novel catalytic activity of castor stearoyl-ACP Delta(9) desaturase. *J Am Chem Soc* 124:3277–3283.
7. Guy JE, Whittle E, Kumaran D, Lindqvist Y, Shanklin J (2007) The crystal structure of the ivy Delta4-16:0-ACP desaturase reveals structural details of the oxidized active site and potential determinants of regioselectivity. *J Biol Chem* 282:19863–19871.
8. Whittle E, Cahoon EB, Subrahmanyam S, Shanklin J (2005) A multifunctional acyl-acyl carrier protein desaturase from Hedera helix L. (English ivy) can synthesize 16- and 18-carbon monoene and diene products. *J Biol Chem* 280:28169–28176.
9. Broadwater JA, Ai J, Loehr TM, Sanders-Loehr J, Fox BG (1998) Peroxodiferric intermediate of stearoyl-acyl carrier protein delta 9 desaturase: Oxidase reactivity during single turnover and implications for the mechanism of desaturation. *Biochemistry* 37:14664–14671.
10. Haas JA, Fox BG (2002) Fluorescence anisotropy studies of enzyme-substrate complex formation in stearoyl-ACP desaturase. *Biochemistry* 41:14472–14481.
11. Moche M, Shanklin J, Ghoshal A, Lindqvist Y (2003) Azide and acetate complexes plus two iron-depleted crystal structures of the di-iron enzyme delta9 stearoyl-acyl carrier protein desaturase. Implications for oxygen activation and catalytic intermediates. *J Biol Chem* 278:25072–25080.
12. Holm L, Rosenstrom P (2010) Dali server: Conservation mapping in 3D. *Nucleic Acids Res* 38:W545–549.
13. Krissinel E, Henrick K (2007) Inference of macromolecular assemblies from crystalline state. *J Mol Biol* 372:774–797.
14. de Vries SJ, van Dijk M, Bonvin AM The HADDOCK web server for data-driven biomolecular docking. *Nat Protoc* 5:883–897.
15. Tremblay AE, Whittle E, Buist PH, Shanklin J (2007) Stereochemistry of Delta4 dehydrogenation catalyzed by an ivy (Hedera helix) Delta9 desaturase homolog. *Org Biomol Chem* 5:1270–1275.
16. Heilmann I, Pidkowich MS, Girke T, Shanklin J (2004) Switching desaturase enzyme specificity by alternate subcellular targeting. *Proc Natl Acad Sci USA* 101:10266–10271.
17. Nguyen HT, et al. (2010) Metabolic engineering of seeds can achieve levels of omega-7 fatty acids comparable with the highest levels found in natural plant sources. *Plant Physiol* 154:1897–1904.
18. Cahoon EB, Lindqvist Y, Schneider G, Shanklin J (1997) Redesign of soluble fatty acid desaturases from plants for altered substrate specificity and double bond position. *Proc Natl Acad Sci USA* 94:4872–4877.
19. Shanklin J (2000) Overexpression and purification of the Escherichia coli inner membrane enzyme acyl-acyl carrier protein synthase in an active form. *Protein Expr Purif* 18:355–360 and correction (2000) 19:319.
20. Leslie AG (1992) Recent changes to the MOSFLM package for processing film and image plate data. *Joint CCP4 + ESF-EAMCB Newsletter on Protein Crystallography*, 26.
21. Evans PR (1993) *Data Collection and Processing* (Daresbury Lab, Warrington, UK), pp 114–122.
22. Winn MD, et al. (2011) Overview of the CCP4 suite and current developments. *Acta Crystallogr D Biol Crystallogr* 67:235–242.
23. Vagin A, Teplyakov A (1997) Molrep: An automated program for molecular replacement. *J Appl Crystallogr* 30:1022–1025.
24. Murshudov GN, Vagin AA, Dodson EJ (1997) Refinement of macromolecular structures by the maximum-likelihood method. *Acta Crystallogr D Biol Crystallogr* 53:240–255.
25. Brunger AT, et al. (1998) Crystallography & NMR system: A new software suite for macromolecular structure determination. *Acta Crystallogr D Biol Crystallogr* 54:905–921.
26. Emsley P, Lohkamp B, Scott WG, Cowtan K (2010) Features and development of Coot. *Acta Crystallogr D Biol Crystallogr* 66:486–501.
27. Laskowski RA, MacArthur MW, Moss DS, Thornton JM (1993) PROCHECK: A program to check the stereochemical quality of protein structures. *J Appl Crystallogr* 26:283–291.
28. Vaguine AA, Richelle J, Wodak SJ (1999) SFCHECK: A unified set of procedures for evaluating the quality of macromolecular structure-factor data and their agreement with the atomic model. *Acta Crystallogr D Biol Crystallogr* 55:191–205.
29. Davis IW, et al. (2007) MolProbity: All-atom contacts and structure validation for proteins and nucleic acids. *Nucleic Acids Res* 35:W375–383.
30. DeLano WL (2002) *The PyMOL Molecular Graphics System* (DeLano Scientific, San Carlos, CA).
31. Whittle EJ, Tremblay AE, Buist PH, Shanklin J (2008) Revealing the catalytic potential of an acyl-ACP desaturase: Tandem selective oxidation of saturated fatty acids. *Proc Natl Acad Sci USA* 105:14738–14743.
32. Broadwater JA, Fox BG (1999) Spinach holo-acyl carrier protein: Overproduction and phosphopantetheinylation in Escherichia coli BL21(DE3), in vitro acylation, and enzymatic desaturation of histidine-tagged isoform I. *Protein Expr Purif* 15:314–326.
33. Cahoon EB, Shanklin J (2000) Substrate-dependent mutant complementation to select fatty acid desaturase variants for metabolic engineering of plant seed oils. *Proc Natl Acad Sci USA* 97:12350–12355.
34. Yamamoto K, Shibahara A, Nakayama T, Kajimoto G (1991) Determination of double-bond positions in methylene-interrupted dienoic fatty acids by GC-MS as their dimethyl disulfide adducts. *Chem Phys Lipids* 60:39–50.